Effects of Cyclometalation on the Panchromatic Ruthenium Sensitizer for DSSC Applications

Ramesh Kumar Chitumalla and Joonkyung Jang*

Department of Nanoenergy Engineering, Pusan National University, Busan 46241, Republic of Korea.
**E-mail: jkjang@pusan.ac.kr*
Received July 24, 2017, Accepted August 10, 2017, Published online September 11, 2017

Ruthenium sensitizers are promising materials for dye sensitized solar cells (DSSCs) and the concept of cyclometalation has been proposed to advance their performance. Density functional theory (DFT) simulations were performed to elucidate the electronic structure, electrochemical, and optical behavior of a cyclometalated ruthenium dye. The cyclometalated sensitizer has superior electrochemical properties (HOMO, LUMO, and bandgap) compared to its non-cyclometalated sensitizer. Upon cyclometalation, a remarkable improvement in the absorption across the UV–Visible and near-infrared regime has been observed. Furthermore, from the electron density contours of frontier molecular orbitals of dye attached TiO_2, the charge transfer and sensitizing properties of the cyclometalated complex are superior to the corresponding non-cyclometalated ruthenium sensitizer. The density of states revealed the strong electronic coupling, which facilitates an effective electron injection into the semiconductor.

Keywords: Dye sensitized solar cell, Ru-sensitizer, Cyclometalation, Density functional theory, Density of states

Introduction

Since the invention of dye sensitized solar cells (DSSCs), the ruthenium sensitizers have been proven to be excellent candidates owing to their extraordinary electrochemical and photophysical properties.[1] The conventional and champion dyes (more efficient, $\eta > 10\%$) in DSSC, such as **N3**, **N749** (black dye), and their derivatives, are equipped with monodentate NCS^- ligands. The labile nature of the NCS^- ligands influences the long-term stability of ruthenium dye and thereby the photovoltaic efficiency of DSSC. This instability caused by labile NCS^- ligands hindered the growth of the photovoltaic market of DSSC over silicon solar cells. A way to avoid or minimize this problem is to replace the NCS^- ligands by bidentate/tridentate ligands.

To improve the efficiency of DSSC, it is indispensable to enhance the light absorption capability and stability of the sensitizers. Many thiocyanate-free ruthenium dyes could not exhibit power conversion efficiencies beyond 10% (champion dye) because of their poor light harvesting capability in the near-infrared (NIR) region (>800 nm).[2] Because of the strong photon flux in the NIR regime, it is important to develop new ruthenium sensitizers, which can harvest light in the NIR region. Wadman *et al.* have reported for the first time that the cyclometalated organo-runthenium complexes with Ru(C^N^N)(N^N^N) conformation show a broader and red-shifted optical absorption compared to the corresponding non-cyclometalated Ru(N^N^N)$_2$ complexes.[3] The red-shifted absorption for cyclometalated ruthenium dye can be attributed to the destabilization of metal t_{2g} orbital, which is caused by the anionic character of the cyclometalated ligand. Several thiocyanate-free cyclometalated ruthenium dyes have been reported to give more than 10% overall power conversion efficiencies.[4]

In the present study, we have chosen a cyclometalated ruthenium complex with Ru(N^C^N)(N^N^N) conformation and its corresponding non-cyclometalated Ru(N^N^N)$_2$ complex. The experimental data of the cyclometalated complex are available.[5] Herein we comprehensively and systematically study the effects of cyclometalation on the structural, electrochemical, and photophysical properties of a ruthenium sensitizer by using the density functional theory (DFT) and the time dependent DFT (TDDFT). The density of states is analyzed to determine the strength of electronic coupling between the dye excited state and the TiO_2 conduction band.

Computational Details

All the electronic structure simulations (DFT/TDDFT) were carried out using Gaussian 09 *ab initio* program.[6] First, the ground state (S_0) structures of the ruthenium dyes (cyclometalated and non-cyclometalated) were optimized in the gas phase by employing the B3LYP[7,8] functional and 6-31G(d,p) basis set. An effective core potential[9] (LanL2DZ) was used for ruthenium. The optimization was performed until the maximum internal force on all the atoms was less than 4.5×10^{-4} eV/Å and the stress was less than 1.01×10^{-3} kbar. The optimized ground state singlet structures *i.e.*, the local minima on the potential energy surface were confirmed by the vibrational frequency analysis ensuring

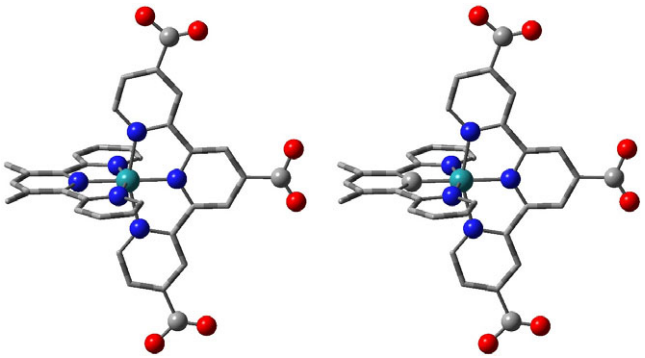

Figure 1. Optimized geometries (S_0) of the dyes **M** (left) and **C** (right) simulated at the B3LYP/6-31G(d,p)/LanL2DZ level of theory.

no imaginary frequencies. We performed population analyses to obtain the electron density distributions in the frontier molecular orbitals (FMOs) of the dyes. The optimized structures were then subject to the TDDFT single point energy simulations to evaluate the optical spectra of the dyes. The first 20 singlet-singlet allowed excitations were used to simulate the spectra in the range of 300–800 nm. We employed the implicit polarizable continuum model[10] to mimic the solvent (DMF) environment in the TDDFT[11] simulation. We also performed the Tamm–Dancoff approximation (TDA)[12] simulations to predict the vibrationally resolved optical absorption spectra.[13] The obtained spectra were then broadened with the Gaussian convolution with a full-width at half maximum of 1500 cm^{-1}.

The dye sensitized semiconductor was modeled by a $(TiO_2)_{16}$ cluster which has been widely used to model the semiconductor.[14] The dye adsorbed (with dissociative bidentate bridging mode) TiO_2 systems were optimized using the B3LYP functional and LanL2DZ basis set. The optimized geometries were then used for the population analyses and TDDFT simulations. The total density of states (TDOS) of dye@TiO_2 and the partial density of states (PDOS) of the dye on TiO_2 were calculated with the help of GaussSum software.[15]

Results and Discussion

Molecular Geometry of the Dyes. The structural information of the dyes is of great help in discussing the charge transfer phenomenon. The molecular geometry of the dyes can also affect the dye aggregation on TiO_2. Considering these points, we have optimized the geometries of the dyes (**M** and **C**) in the gas phase and the resulting geometries are depicted in Figure 1. The two ruthenium dyes have an octahedral (pseudo) geometry around the ruthenium center in which the two ligands (*i.e.*, ancillary and anchoring

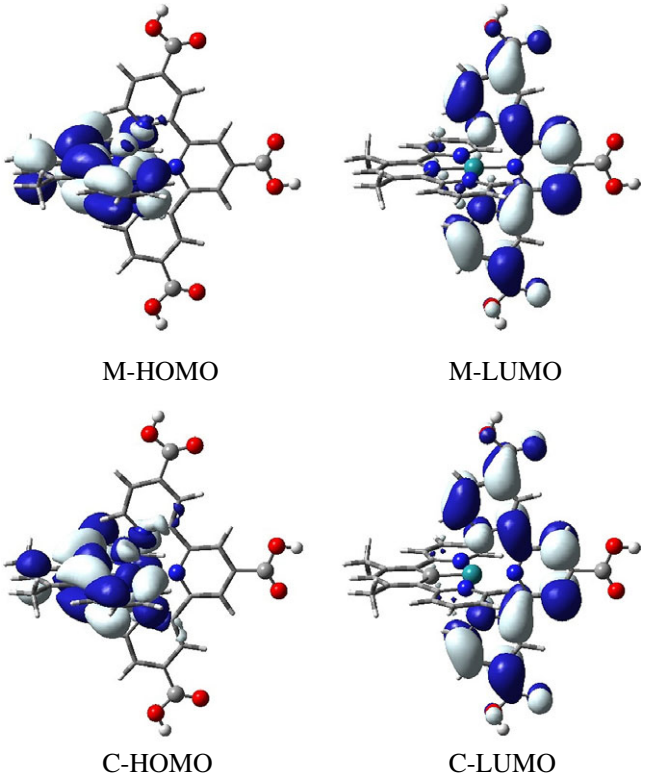

Figure 2. Electron density surface plots of the frontier molecular orbitals of the dyes **M** and **C**.

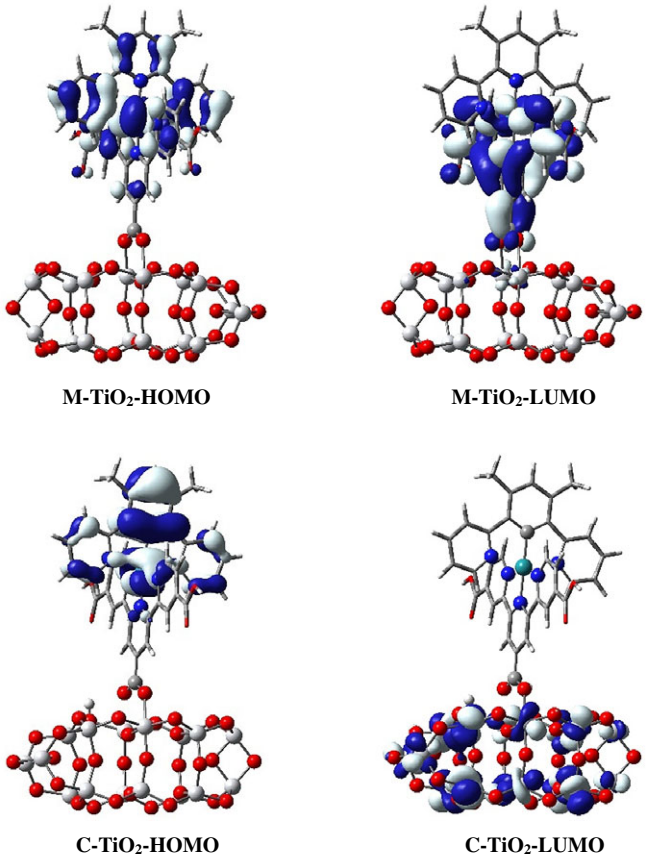

Figure 3. Electron density transfer from the dye to TiO_2 nanocrystal upon photoexcitation. Comparison between non-cyclometalated (top) and cyclometalated (bottom) ruthenium dyes.

Table 1. Simulated electrochemical data of the dyes (**M** and **C**) and dye sensitized TiO_2 (**M**@TiO_2 and **C**@TiO_2) in a DMF solvent.

	HOMO (eV)	LUMO (eV)	HLG (eV)[a]	E_{0-0} (eV)[b]
M	−6.39	−3.21	3.18	2.29
C	−5.35	−2.85	2.50	1.66
M@TiO_2	−6.43	−3.46	2.97	2.12
C@TiO_2	−5.54	−3.26	2.28	1.54

[a] HLG = HOMO–LUMO gap.
[b] $S_0 \rightarrow S_1$ excitation energy.

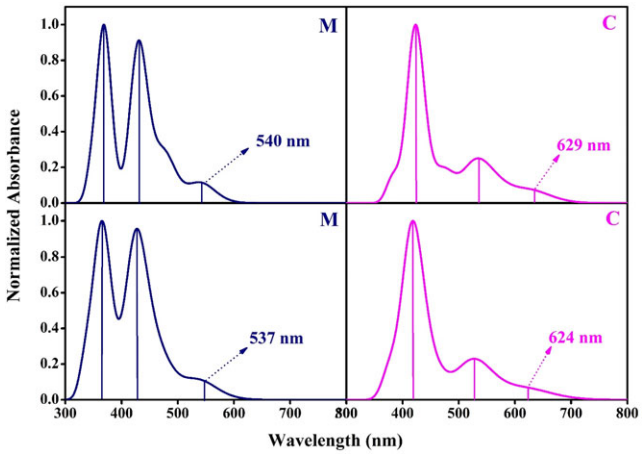

Figure 4. UV–Visible absorption spectra of the dyes **M** (left) and **C** (right) in a DMF solvent obtained by using the TDDFT (top) and Tamm–Dancoff approximation (bottom).

ligands) are almost perpendicular to each other. The complexes **M** and **C** are di-cationic and mono-cationic, respectively. The Ru–C bond distance (cyclometalated bond in **C**) is 1.99 Å and the corresponding bond distance in **M** is 2.04 Å. The other Ru–N bond distances are *ca.* 2.10 Å and not varied significantly from **M** to **C**. Notice that the cyclometalation do not produce any substantial changes in the structural parameters.

The calculated dipole moments are 8.58 and 3.02 Debye for **M** and **C**, respectively. The decrease in the dipole moment for **C** can be attributed to the decreased net charge of the complex. To study the adsorption behavior of the dyes on TiO_2, we carried out the adsorption of the two dyes on a 16 unit TiO_2 cluster, $(TiO_2)_{16}$. The bond distances between carboxylic oxygen atoms (two) of the dye and Ti atoms of the TiO_2 cluster are 2.12 and 2.21 Å for **M** and 2.09 and 2.19 Å for **C**, respectively. The shortened bond distances for **C** reveals its stronger adhering nature with TiO_2 than that of **M**.

Electrochemical Properties. We carried out the molecular orbital analysis on the optimized geometries of the dyes and dye attached TiO_2. The isodensity (isovalue = ±0.02 e $Å^{-3}$) surfaces of the FMOs are shown in Figure 2 (dyes) and Figure 3 (dye sensitized TiO_2). The electron densities in the HOMOs of the dyes center on the ancillary ligand and ruthenium center, whereas in the LUMOs, the electron density is transferred to the anchoring ligand. In Figure 2, the electron density distributions for the both dyes are similar. The simulated electrochemical data obtained in the DMF solvent are listed in Table 1. The HOMOs of the dyes have energies of −6.39 and −5.35 eV and LUMOs −3.21 and −2.85 eV for **M** and **C**, respectively. Both the HOMO and LUMO were destabilized from **M** to **C** due to the stabilization of ruthenium center upon cyclometalation.[16] The observed destabilization in the HOMO and LUMO is nonuniform, and the higher destabilization of HOMO than that of LUMO (by 0.68 eV) resulted in a decreased HOMO–LUMO gap (HLG) of **C**. A considerable bathochromic shift in the optical absorption spectrum of **C** is expected due to the decreased HLG. The HOMO and LUMO levels of the dyes satisfy the DSSC requirement: *i.e.*, the simulated HOMO level is below the redox potential of redox couple I^-/I_3^- and the LUMO level is above the conduction band of the TiO_2.

The charge transfer phenomenon in the dye sensitized TiO_2 plays a key role in the DSSC mechanism. Figure 3 shows that a more charge has been transferred to TiO_2 from

Table 2. Simulated optical data of the dyes **M** and **C** by using the TDDFT and TDA methods at B3LYP/6-31G(d,p)/LanL2DZ level.

Dye	λ (nm)	Bandgap E_{0-0} (eV)	Excitation state	Oscillator strength (*f*)	LHE	Predominant transition
M (TD)	540	2.29	$S_0 \rightarrow S_1$	0.0447	0.098	HOMO→LUMO (98%)
	476		$S_0 \rightarrow S_3$	0.1062	0.217	H-2→LUMO (77%)
	445		$S_0 \rightarrow S_4$	0.0122	0.028	HOMO→L + 2 (90%)
C (TD)	629	1.66	$S_0 \rightarrow S_2$	0.0514	0.112	H-2→LUMO (93%)
	566		$S_0 \rightarrow S_4$	0.0701	0.149	H-1→LUMO (73%)
	529		$S_0 \rightarrow S_5$	0.1620	0.311	H-1→L + 1(97%)
M (TDA)	537	2.31	$S_0 \rightarrow S_1$	0.0462	0.101	HOMO→LUMO (97%)
	470		$S_0 \rightarrow S_3$	0.0894	0.186	H-2→LUMO (67%)
	443		$S_0 \rightarrow S_4$	0.0133	0.030	HOMO→L + 2 (86%)
C (TDA)	624	1.67	$S_0 \rightarrow S_2$	0.0510	0.111	H-2→LUMO (92%)
	555		$S_0 \rightarrow S_4$	0.0469	0.102	H-1→LUMO (60%)
	524		$S_0 \rightarrow S_5$	0.1737	0.330	H-1→L + 1 (96%)

C than from **M** upon photo excitation. Hence, the cyclometalated dye **C** is more efficient in charge injection compared to that of non-cyclometalated dye **M**. Both the HOMO and LUMO of the dye sensitized TiO_2 have been stabilized compared to those of respective isolated dyes. The HLG reduced by *ca*. 0.2 eV for the both dyes upon their adsorption on TiO_2.

Optical Properties. We simulated the UV–Visible absorption spectra of the dyes in a DMF solvent by using the TDDFT and Tamm–Dancoff approximated TDDFT (TDA) formalisms (Figure 4). The corresponding optical properties are listed in Table 2. The spectra obtained from TDA method have shown small 3–5 nm hypsochromic shifts but the shape and number of the bands have not varied significantly from those obtained from the TDDFT method. The absorption maxima of the dyes in the low-energy region arises from the metal-to-ligand charge transfer transition. The calculated TDDFT absorption maxima are 540 and 629 nm for **M** and **C**, respectively. These intense low-energy transitions predominantly arise from the HOMO➔LUMO for **M** and HOMO-2➔LUMO for **C**. The bathochromic shift of *ca*. 90 nm upon cyclometalation originates from the decreased HLG (*vide supra*).

The cutoff wavelength beyond which there is no absorption, $\lambda_{cutoff,}$ extends up to *ca*. 750 nm for **C** while only up to *ca*. 620 nm for **M** in both the TDDFT and TDA calculations. The 0–0 energies (E_{0-0}) of **M** and **C** obtained from the TDDFT method are 2.29 and 1.66 eV, which are not significantly different from those, obtained using the TDA method. The light harvesting efficiencies (LHEs) of **C** are more than those of **M** calculated at various wavelengths. The ground to excited state dipole moments are 18.11 and 11.88 Debye for **M** and **C**, respectively. The larger dipole moments of the dyes compared to the ground state dipole moments originate from the bathochromic shift in a polar solvent.

To gain deeper insights into the vertical excitation energies of the dye sensitized TiO_2, we performed the TDDFT simulations of the dye@TiO_2 systems. The simulated absorption maxima are 585 and 686 nm for **M** and **C**, respectively. The bathochromic shift of 101 nm for C@TiO_2 from that of M@TiO_2 can be attributed to the decreased HLG by 0.69 eV. A considerable bathochromic shift (*ca*. 50 nm) has been observed for dye@TiO_2 compared to an isolate dye.

Density of States. We calculated the density of states (DOS) for the bare (pristine) TiO_2 and the dyes adsorbed TiO_2 from their optimized geometries. Figure 5 shows the TDOS of the bare TiO_2 along with the TDOS of TiO_2 after adsorption of **M** and **C**. In the same figure, the PDOSs of the dyes are depicted as well. In Figure 4(a), one can see that the valence and conduction bands of the bare TiO_2 are separated by a wide bandgap (>4 eV). On the other hand, the DOS of the dye sensitized TiO_2 shows a decreased bandgap due to the sharply occupied molecular orbitals (HOMOs) of the dye. In the case of C@TiO_2, the HOMO is destabilized from that of M@TiO_2 by 0.89 eV. The energetic overlap of the dye excited state (LUMO) with the TiO_2 conduction band determines the electron injection from dye to TiO_2, and there by the overall performance of DSSC. From the DOS analysis, the excited states of both

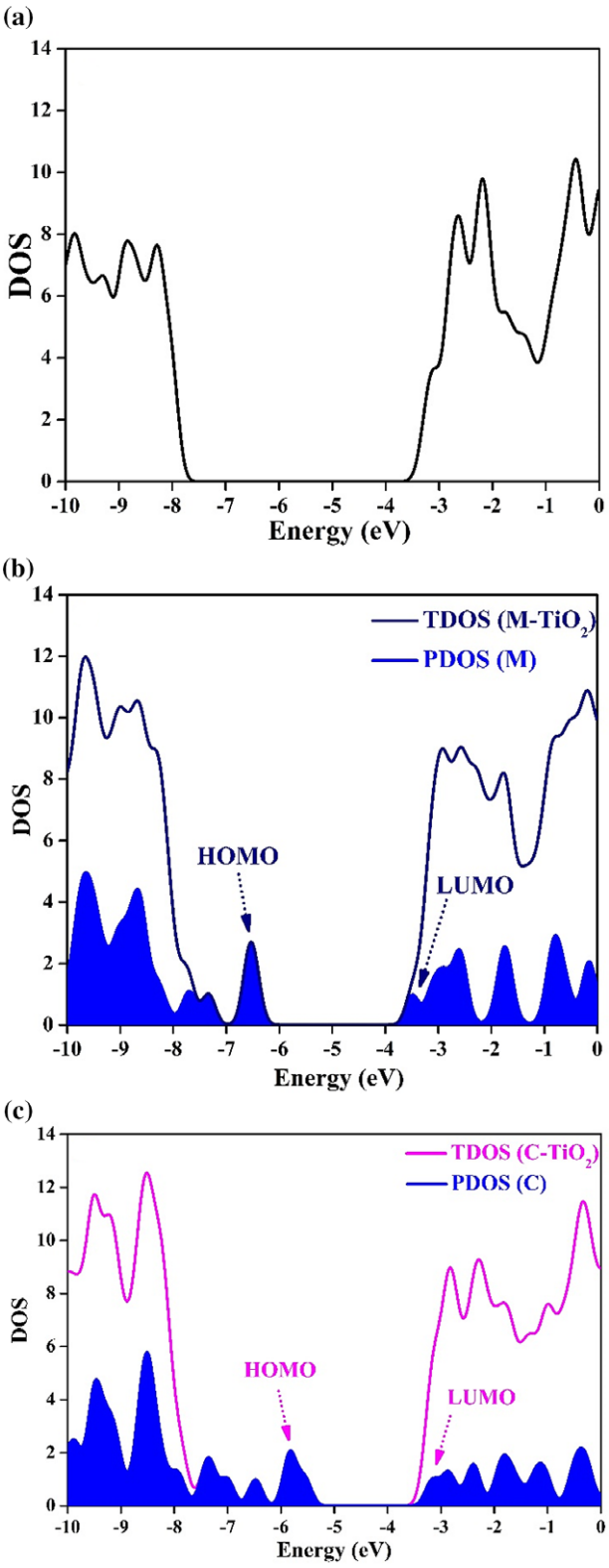

Figure 5. Density-of-state plots of (a) the bare TiO_2 cluster, (b) M-TiO_2, and (c) C-TiO_2.

dyes have strong energetic overlaps with the TiO_2 conduction band. The wider broadening of the LUMO (Figure 4 (c)) of dye **C** signifies the stronger electronic overlap and a more effective electron injection into the TiO_2 conduction band than those of **M**.[14]

Conclusion

The present DFT/TDDFT study indicates that the cyclometalated organo-ruthenium complex has improved electrochemical and optical properties for DSSC applications compared to the corresponding non-cyclometalated ruthenium polypyridyl complex. The cyclometalated ruthenium complex has shown an approximately 100 nm red-shift in the UV–Visible absorption and the λ_{cutoff} reached 750 nm. The LHEs calculated at different wavelengths for cyclometalated dye are better than those of non-cyclometalated dye. The population analysis and DOS revealed that the cyclometalated dye has stronger electron injection capability into the semiconductor over non-cyclometalated dye.

Acknowledgments. This study was financially supported by the 2016 Post-Doc. development program of Pusan National University and by the National Research Foundation of Korea (NRF) grant funded by the Korean government (NRF-2016H1D3A1936765).

References

1. B. O'Regan, M. Grätzel, *Nature* **1991**, *353*, 737.
2. K.-L. Wu, H.-C. Hsu, K. Chen, Y. Chi, M.-W. Chung, W.-H. Liu, P.-T. Chou, *Chem. Commun.* **2010**, *46*, 5124.
3. S. H. Wadman, J. M. Kroon, K. Bakker, M. Lutz, A. L. Spek, G. P. M. van Klink, G. van Koten, *Chem. Commun.* **2007**, 1907–1909.
4. T. Bessho, E. Yoneda, J.-H. Yum, M. Guglielmi, I. Tavernelli, H. Imai, U. Rothlisberger, M. K. Nazeeruddin, M. Grätzel, *J. Am. Chem. Soc.* **2009**, *131*, 5930.
5. R. K. Chitumalla, K. S. V. Gupta, C. Malapaka, R. Fallahpour, A. Islam, L. Han, B. Kotamarthi, S. P. Singh, *Phys. Chem. Chem. Phys.* **2014**, *16*, 2630.
6. M. J. Frisch, G. W. Trucks, H. B. Schlegel, G. E. Scuseria, M. A. Robb, J. R. Cheeseman, G. Scalmani, V. Barone, B. Mennucci, G. A. Petersson, et al., *Gaussian09, Revision D. 01*, Gaussian, Inc, Wallingford, CT, **2013**.
7. A. D. Becke, *J. Chem. Phys.* **1993**, *98*, 5648.
8. A. D. Becke, *J. Chem. Phys.* **1996**, *104*, 1040.
9. P. J. Hay, W. R. Wadt, *J. Chem. Phys.* **1985**, *82*, 270.
10. M. Cossi, V. Barone, R. Cammi, J. Tomasi, *Chem. Phys. Lett.* **1996**, *255*, 327.
11. R. Bauernschmitt, R. Ahlrichs, *Chem. Phys. Lett.* **1996**, *256*, 454.
12. R. Cammi, B. Mennucci, J. Tomasi, *J. Phys. Chem. A* **2000**, *104*, 5631.
13. S. Hirata, M. Head-Gordon, *Chem. Phys. Lett.* **1999**, *314*, 291.
14. M. Paramasivam, R. K. Chitumalla, S. P. Singh, A. Islam, L. Han, V. Jayathirtha Rao, K. Bhanuprakash, *J. Phys. Chem. C* **2015**, *119*, 17053.
15. N. M. O'Boyle, A. L. Tenderholt, K. M. Langner, *J. Comput. Chem.* **2008**, *29*, 839.
16. S. Fantacci, F. De Angelis, A. Sgamellotti, N. Re, *Chem. Phys. Lett.* **2004**, *396*, 43.

